frontiers | Frontiers in Marine Science

ORIGINAL RESEARCH
published: 26 April 2022
doi: 10.3389/fmars.2022.855009

# Competitive Interactions Between Microbial Siderophores and Humic-Like Binding Sites in European Shelf Sea Waters

*Martha Gledhill*[1]*, *Kechen Zhu*[1], *Dagmara Rusiecka*[1,2] *and Eric P. Achterberg*[1]

[1] GEOMAR, Helmholtz Centre for Ocean Research, Kiel, Germany, [2] Ocean and Earth Science, National Oceanography Centre, University of Southampton, Southampton, United Kingdom

Siderophores are low molecular weight high affinity iron chelates found at low concentrations in seawater. In this study we determined the total concentrations and identities of siderophores in extracts isolated from a shelf sea environment on the Northwest European shelf by high performance liquid chromatography coupled to high resolution inductively coupled plasma mass spectrometry (ICP-MS) in parallel to high resolution electrospray ionisation mass spectrometry (ESI-MS). We identified a total of 24 different siderophores in our samples *via* metal isotope profiling of masses detected by ESI-MS. Twenty three of the identified siderophores could be assigned to three siderophore families – ferrioxamines, amphibactins and marinobactins. In contrast, only 12 peaks could be resolved in iron chromatograms obtained *via* ICP-MS analysis. Comparison of results obtained by the two mass spectrometry detectors showed that neither method was able to detect and identify all siderophores present in the samples on its own. We assessed the impact of our observed total siderophore concentrations on iron speciation by calculating the distribution of iron species as a function of total siderophore concentrations at different iron concentrations representative of our study area. We considered competition for iron between siderophores, a humic like dissolved organic matter (DOM) fraction and hydroxide ions by combining an ion-pair model with a non-ideal competitive interaction (NICA)-Donnan model. We found that the overall impact of siderophores on iron biogeochemistry is low at concentrations of siderophore <100 pmol $L^{-1}$, and that the dominant iron species present at siderophore concentrations of the order of a few tens of pmol $L^{-1}$ will be iron bound to the humic like DOM fraction. Furthermore the heterogeneity of binding sites in the humic like DOM fraction means that other binding sites present in organic matter could be effective competitors for siderophores, especially at low iron concentrations. Our findings highlight the importance of binding site heterogeneity when considering the influence of different iron binding groups on iron speciation in the marine environment.

**Keywords: iron, chemical speciation, NICA model, liquid chromatography mass spectrometry, ICP- MS**

OPEN ACCESS

***Edited by:***
*Marta Plavsic,*
*Rudjer Boskovic Institute, Croatia*

***Reviewed by:***
*Rene Boiteau,*
*Oregon State University, United States*
*Daniel James Repeta,*
*Woods Hole Oceanographic Institution, United States*

***Correspondence:**
*Martha Gledhill*
*mgledhill@geomar.de*

***Specialty section:***
*This article was submitted to Marine Biogeochemistry, a section of the journal Frontiers in Marine Science*

***Received:*** *14 January 2022*
***Accepted:*** *30 March 2022*
***Published:*** *26 April 2022*

***Citation:***
*Gledhill M, Zhu K, Rusiecka D and Achterberg EP (2022) Competitive Interactions Between Microbial Siderophores and Humic-Like Binding Sites in European Shelf Sea Waters. Front. Mar. Sci. 9:855009. doi: 10.3389/fmars.2022.855009*

## INTRODUCTION

Iron is an essential micronutrient for pyhtoplankton growth, but its low solubility in oxygenated water results in sub nanomolar concentrations (Liu and Millero, 2002) which limit productivity in approximately 30-40% of the surface ocean (Boyd and Ellwood, 2010; Hutchins and Boyd, 2016). Siderophores are secondary metabolites produced by bacteria and fungi in order to acquire iron (Hider and Kong, 2010) and are thought to make up a component of the dissolved iron pool in seawater, likely influencing iron bioavailability to marine microbes (Shaked and Lis, 2012; Hogle et al., 2021). More than forty siderophores from marine bacteria have been characterised (Vraspir and Butler, 2009) and four groups of these siderophores, ferrioxamines, amphibactins, synechobactins and petrobactins have been shown to occur in open ocean surface waters (Mawji et al., 2008; Boiteau et al., 2016; Velasquez et al., 2016; Bundy et al., 2018; Manck et al., 2021). The concentrations of individual siderophores have been determined to be of the order of a few picomoles per litre (Mawji et al., 2008; Bundy et al., 2018; Boiteau et al., 2019), similar in magnitude to other microbial exatometabolites (i.e. extracellular metabolites) such as vitamins (Sañudo-Wilhelmy et al., 2012), and potentially higher than forms of iron (e.g. iron(III) hydroxide ions), known to be more widely bioavailable to marine phytoplankton (Bundy et al., 2018). In general, the low quantity of data on siderophore distributions in the ocean means there is currently limited information on the variety and abundance of siderophores in marine systems. Furthermore, given that the concentrations of siderophores observed are generally low relative to the total dissolved iron concentration, and the overall concentration of iron binding ligands (Boiteau et al., 2016; Buck et al., 2018; Bundy et al., 2018) the role that these compounds play in the biogeochemical cycling of iron in the ocean is not well understood.

The impact of siderophores on iron biogeochemistry is likely influenced by the presence of other iron binding compounds present in seawater such as humic substances (Laglera et al., 2007; Gledhill and Buck, 2012; Slagter et al., 2017; Whitby et al., 2020). Recent work has confirmed that binding site distributions in marine dissolved organic matter are heterogeneous and thus like those of humic substances (Hiemstra and van Riemsdijk, 2006; Lodeiro et al., 2020; Lodeiro et al., 2021; Zhu et al., 2021a; Zhu et al., 2021b). The total concentration of binding sites in the portion of marine DOM that can be extracted from seawater by hydrophobic resins at pH 2 approximates 130 mmol $mol^{-1}$ C (Lodeiro et al., 2020; Lodeiro et al., 2021). At least 10% of C atoms are therefore bonded to a heteroatom with an available proton binding group and the total proton binding site concentration in seawater can be estimated to be of the order of a few μmol $L^{-1}$. Proton affinities for marine DOM follow a bimodal distribution as observed for humic substances including fulvic and humic acids, although analysis to date suggests that marine DOM is likely less heterogeneous than terrestrial fulvic and humic acids (Lodeiro et al., 2020; Lodeiro et al., 2021; Zhu et al., 2021a; Zhu et al., 2021b). The heterogeneity of marine DOM means that a small portion of the many binding sites present likely have structures favourable for formation of relatively stable iron complexes *via* e.g., the chelate effect (Fraústo Da Silva, 1983) and has implications for assessing competitive interactions between ions (Tipping, 1993). The importance of heterogeneity for building a full understanding of competitive interactions between cations was first highlighted nearly forty years ago (e.g., Perdue and Lytle, 1983) and formed the basis for the development of continuous binding site distribution models commonly applied to investigations of metal binding to humic substances (Perdue and Lytle, 1983; Kinniburgh et al., 1996; Tipping et al., 2011). However, heterogeneity also has implications for interactions between different ligand groups, especially those such as siderophores that are specifically produced by microbes, have a high affinity for iron but are present at relatively low abundance. Nevertheless, to our knowledge, competition between siderophores and humic substance-like binding sites in marine DOM, has not previously considered the impact of this heterogeneity.

In this study we combine high performance liquid chromatography (HPLC) with high resolution electrospray ionisation mass spectrometry (ESI-MS) and inductively coupled mass spectrometry (ICP-MS) to identify and quantify siderophores in the Celtic Sea on the Northwest European Shelf. We used the range of determined siderophore concentrations to further assess the competition between siderophores and a humic substance-like component of DOM, which was investigated on the same cruises in parrallel to this study (Zhu et al., 2021a). We therefore add complexation of siderophores to the non-ideal competitive adsorption (NICA) model developed in Zhu et al. (2021a) and calculate the resultant species distributions as function of increasing siderophore concentration in order to improve understanding of the impact of siderophore production on iron speciation in our study area (Birchill et al., 2017; Poulton et al., 2017; Davis et al., 2018).

Our study was undertaken as part of the UK Shelf Sea Biogeochemistry program investigating the role of the shelf sea in carbon sequestration and the seasonal dynamics of trace elements, including iron, at the shelf edge. Recent work has demonstrated strong seasonal cycling of both iron and carbon in the Celtic Sea. High productivity in the spring results in the drawdown of nitrate, phosphate and iron to concentrations similar to those in nutrient limited regions of the open ocean (Birchill et al., 2017). Although dissolved organic carbon concentrations in the Celtic Sea do not have a strong seasonal cycle (Davis et al., 2018; Wihsgott et al., 2019), the shelf environment experiences both spring and autumn phytoplankton blooms, which could influence siderophore production *via* changes in bacterial productivity.

## METHODS

Sampling was conducted on three cruises on the *RRS Discovery* in the Celtic Sea in November 2014, April 2015 and July 2015. Siderophore samples were collected from two stations – CCS which was situated on the shelf in the central Celtic Sea, and CS2

which was close to the shelf edge (**Figure 1**; Birchill et al., 2017; Rusiecka et al., 2018). We present data obtained for CCS from all three cruises and for CS2 from the November 2014 cruise. Samples for siderophore identification were obtained from 20 L Niskin bottles mounted on a stainless steel rosette equipped with a conductivity-temperature-depth profiler. A total of 13 to 17 L seawater was sampled into acid washed Nalgene carbuoys. The water was filtered (0.2 µm, Sartobran cellulose acetate filter) immediately prior to solid phase extraction (SPE; 300 mg, 6 mL Env+, Biotage) at a flow rate of 3 mL $min^{-1}$ using a peristaltic pump. Cartridges were air dried and then frozen at -20°C for later extraction and analysis in the laboratory. In November, sample preconcentrations took place at room temperature (ca. 20°C), whilst in April and July, samples were processed in a temperature controlled room at 4°C. Since preconcentration took four days, the microbial population in the November samples could have grown during the preconcentration period with consequent impacts on siderophore concentrations. We therefore only present qualititative information for samples collected in November. Future studies could avoid this potential for bias during preconcentration by filtering the sample prior to collection in the sample reservoir used for preconcentration, preconcentrating at 4°C, or reducing the time required for preconcentration by e.g., increasing the flow rate or reducing the volume preconcentrated.

Once defrosted, cartridges were washed with 5 mL 11 mmol $L^{-1}$ ammonium carbonate to remove inorganic salts, and siderophores were eluted with 5 mL 80:15:5 (v:v:v) acetonitrile:isopropanol:$H_2O$ containing 5 mmol $L^{-1}$ ammonium formate. High purity water (18.2 mΩ$cm^{-1}$, Milli-Q, Millipore), and LC-MS grade solvents and ammonium formate (Fisher) were used throughout, and all sample processing took place under a class 1000 laminar flow hood. A 1 mL aliquot of sample was pipetted into a microcentrifuge tube (Eppendorf, Millipore) and the solvents evaporated under vacuum to near dryness (<100 µL) using a centrifugal evaporator (Thermo). Samples were then diluted to a total volume of 1 mL with 5 mmol $L^{-1}$ ammonium formate prior to analysis.

We analysed each sample three times: 1) after overnight equilibration with added gallium (100 µg $mL^{-1}$ gallium; ICP-MS standard solution) to identify putative siderophores 2) after overnight equilibration with added iron (100 nmol $L^{-1}$ $FeCl_3$) to confirm that gallium complexes could be detected as their corresponding iron complexes and 3) without any metal addition to quantify siderophores present in samples (Mawji et al., 2011).

For identification of siderophores [analyses (1) and (2)], samples were analysed by HPLC-ESI-MS (Biocompatible Ultimate 3000, Orbitrap Q Exactive, Thermo). Separation was performed using a linear gradient from $H_2O$:methanol:formic acid (95:5:0.1 v:v:v) to 100:0.1 methanol:formic (v:v) acid over 10 minutes, at a flow rate of 400 µL $min^{-1}$ with a C18 column (Agilent Zorbax Eclipse Plus, 1.8 × 50 mm, 1.8 µm). The injection volume was 25 µL. We used a peak height cut off of $1 \times 10^5$ ion counts for detection of ESI-MS peaks. Chelomex (Baars et al., 2014) was used to mine ESI-MS data for peaks with gallium isotopes, after converting RAW files to mzXML files with MS Convert (Proteowizard). Iron complexes were subsequently identified in mzmine v2.53 (Pluskal et al., 2010) as described in Gledhill et al. (2019).

For siderophore quantification [analysis (3)], samples were analysed by HPLC-ESI-MS/ICP-MS (Biocompatible Ultimate 3000, Orbitrap Q Exactive, Element XR, Thermo). Both HPLC

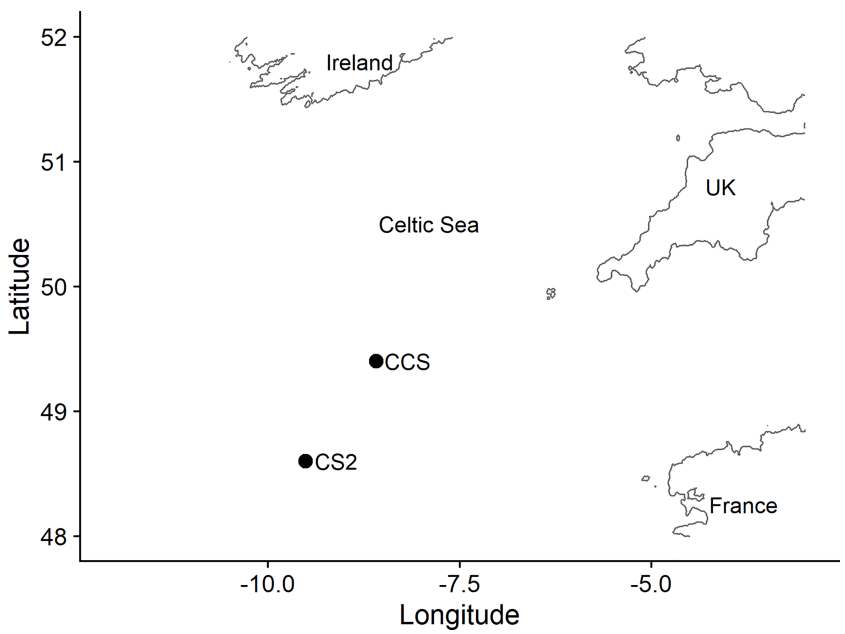


**FIGURE 1** | Map of the study area showing the positions on the two stations in the Celtic Sea.

solvents were modified with 5 mmol $L^{-1}$ ammonium formate and we used a polymeric PEEK column (Hamilton, PRP, 2.1 × 150 mm, 5 µm) in order to reduce background ion counts in the ICP-MS (Boiteau et al., 2013). We used a flow rate of 400 µL $min^{-1}$ and extended the time of the linear gradient of 95:5 $H_2O$: methanol to 100% methanol to 15 minutes to improve peak separation. Immediately after the HPLC column, the flow was split so that 200 µL $min^{-1}$ flowed in parallel to the ESI-MS detector (Orbitrap Q Exactive, Thermo) and ICP-MS detector (Element XR, Thermo). The fraction of eluate going to the ICP-MS detector was dried with a desolvator (Aridus, CETAC) and oxygen added to nebulizer gas at a flow rate of 35 mL $min^{-1}$ to prevent the build-up of carbon on the platinum skimmer cones of the ICP-MS (Boiteau et al., 2013). We monitored the $^{56}Fe$ peak to detect siderophores and $^{59}Co$ to detect cobalamin. Quantification was based on a calibration constructed using standard solutions of ferrioxamine B (Sigma). Ferrioxamine E and G standards (EMC microcollections) were also analysed to confirm retention times. Cobalamin was added as an internal standard to each sample immediately prior to analysis at a concentration of 7.5 nmol $L^{-1}$ to allow for peak alignment (Boiteau et al., 2013). We did not account for changes in ICP-MS sensitivity over the course of the chromatogram (Boiteau et al., 2013). We estimated a detection limit for iron peaks of 1.3 nmol $L^{-1}$ for the preconcentrated sample, based on integration of the noise observed on analysis of extracts of blank SPE cartridges over a 30 second time period (3 × standard deviation of the integrated noise, n=9). Since samples were preconcentrated by at least a factor of 1700 depending on the sample, this can be extrapolated to a detection limit of ca. 0.5 pmol $L^{-1}$ for siderophore concentrations in the original sample.

The potential impact of siderophores on the relative abundance of inorganic iron, iron bound to a humic substance like fraction and the formation of solid iron hydroxide phases was calculated by combining an ion-pair model with the non-ideal competitive adsorption (NICA) - Donnan model (Kinniburgh et al., 1996) within the speciation programme ORCHESTRA (Meeussen, 2003). We used the model as applied in Zhu et al. (2021a), and consider marine DOM as a heterogeneous pool of binding sites analogous to fulvic acid. To describe iron binding to organic matter, we used generic parameters from Milne et al., (2001; 2003) combined with the NICA iron parameters (**Supplementary Table 1**) optimized for the Celtic Sea (Zhu et al., 2021a). We use a single dissolved organic carbon concentration of 47 µmol $L^{-1}$ since scaling binding site concentrations with DOC concentrations had a minor impact on the calculated speciation in our study area (Zhu et al., 2021a). Formation of solid iron hydroxide phases was determined by allowing any free iron ($Fe^{3+}$) in excess of its solubility to precipitate as $Fe(OH)_3(s)$ according to the solubility constants from Liu and Millero (1999). We assumed all siderophores had thermodynamic constants similar to ferrioxamine B (Schijf and Burns, 2016), since thermodynamic stability constants with major ions and even iron are unavailable for most of the siderophores identified in this study. We added thermodynamic constants for ferrioxamine B to the MINTEQ4 database used in ORCHESTRA. We calculated speciation at a fixed pH (8.25 on the NBS scale) and temperature (12°C) since temperature and pH varied by ±1°C and 0.1 pH unit respectively in our study area (Zhu et al., 2021a). Input and output files required for the calculations are available at dx.doi.org/10.17504/protocols.io.b27xqhpn, together with a protocol for calculating iron speciation using ORCHESTRA.

Further data processing, statistical analysis and graphical presentation was carried out in R (R Development Core Team, 2016).

# RESULTS AND DISCUSSION

## Siderophores Identified in Northwest European Shelf Sea Waters

We identified 24 siderophores in preconcentrated samples collected at two stations (**Figure 1**) on the European shelf in the autumn, spring and summer seasons (Nov 2014, April 2015 and July 2015) using ESI-MS. Our criteria were based on the ability of the siderophores to exchange iron with gallium (McCormack et al., 2003), and positive identification required: 1) co-elution of peaks corresponding to complexes with both gallium isotopes ($[M\text{-}2H+^{69}Ga]^+$ and $[M\text{-}2H+^{71}Ga]^+$, Δm/z=1.995) and $^{71}Ga$:$^{69}Ga$ peak areas with ratios that reflected the natural isotopic composition of Ga (i.e. ratio within 0.66 ± 0.19) and 2) elution of a peak corresponding to the $[M\text{-}2H+^{56}Fe]^+$ isotope in the absence of gallium. We used the exact mass, isotopic ratios of $^{12}C$:$^{13}C$ and retention times to identify hydroxamate siderophores of the ferrioxamine and amphibactin families, according to the seven golden rules criteria (Kind and Fiehn, 2007) and *via* comparison with previous work (McCormack et al., 2003; Gledhill et al., 2004; Mawji et al., 2011). The identities of ferrioxamines E and G were unequivocally confirmed by direct comparison with standards.

Based on exact mass, we were able to tentatively identify ferrioxamines G2 and D2 in marine samples for the first time. Ferrioxamines are synthesized by the non-ribosomal peptide independent synthase pathway, and all four of these siderophores could potentially be produced by the same bacteria (Ronan et al., 2018). We identifed 7 structurally characterised amphibactins (Martinez and Butler, 2007) which have been found in offshore Pacific surface waters (Boiteau et al., 2016) and identifed in incubations from Atlantic waters (Mawji et al., 2011). We also identified 4 previously characterized marinobactins (Martinez et al., 2000). To our knowledge, this is the first report for the isolation of marinobactins from seawater samples, although they were amongst the first marine siderophores to be characterised from bacterial isolates.

We predicted molecular formulas for unknown siderophores by extension of fatty acid chain length, or addition of further functional groups commonly associated with siderophores (e.g., hydroxyl group). We used the number of predicted nitrogen atoms in the formulae to group our siderophores into families. Thus, five of our unknowns belong to the $N_7$ family (m/z = 915.4265, 921.4141, 937.4089, 945.4350) which included the amphibactins, and three to the $N_9$ family (m/z= 957. 374, 1045.424, 1059.405) which contained the marinobactins. One

of our $N_9$ siderophores (m/z = 1045.424) could also have been previously identified in an incubated surface seawater from the South Atlantic Ocean (Mawji et al., 2011). Plots of retention times *vs* mass/charge ratio (**Figure 2**) clustered the siderophores into different groups broadly aligned with our familial assignments. Although molecular weight was the dominant factor influencing retention time, increases in the number of oxygen atoms, which were potentially associated with further hydroxylation of the fatty acid chain, resulted in decreased retention times, consistent with likely decreased hydrophobicity. Thus, under our chromatographic conditions, the ferrioxamine siderophores were the most hydrophilic, eluting at retention times between the solvent front and 4 minutes, $N_9$ siderophores eluted between 5.5 and 8.6 minutes and $N_7$ siderophores between 8.6 and 9.6 minutes (**Figure 2**). The chromatographic behaviour thus suggests $N_9$ are more hydrophilic than $N_7$ siderophores, even though they have higher molecular masses. Hydrophobicity of siderophores likely impacts on their biogeochemical behaviour in the environment, since it influences cell-water partitioning. For example, hydrophobic siderophores have been isolated from the cells of bacteria, rather than from the culture media (Xu et al., 2002; Martinez et al., 2003). Furthermore association of siderophores with cell surfaces or particles could point to a more important role for these compounds in remineralisation processes (Bundy et al., 2014; Velasquez et al., 2016).

Predicted formulas for three of the unknown $N_7$ siderophores had odd numbers of carbon atoms and these $N_7$ siderophores were therefore not linked directly to structurally characterised amphibactins (Martinez et al., 2003) *via* extension of fatty acid chains since fatty acid chains typically increase by n=2. However, the abundances of these three $N_7$ unknowns significantly correlated with amphibactins D and E ($r>0.9$, $p<0.01$, n=6-7) suggesting a close environmental association between the two types of siderophores and a common producing bacterium cannot be ruled out. Many bacteria can produce and utilise more than one kind of siderophore (Lee et al., 2012).

We were unable to assign a formula to the siderophore identified with m/z 958.505. This siderophore could not thus be linked with the other siderophore groups based on the molecular characteristics alone, although the chromatographic behaviour suggests that this compound may also be associated with the amphibactins (**Figure 2**).

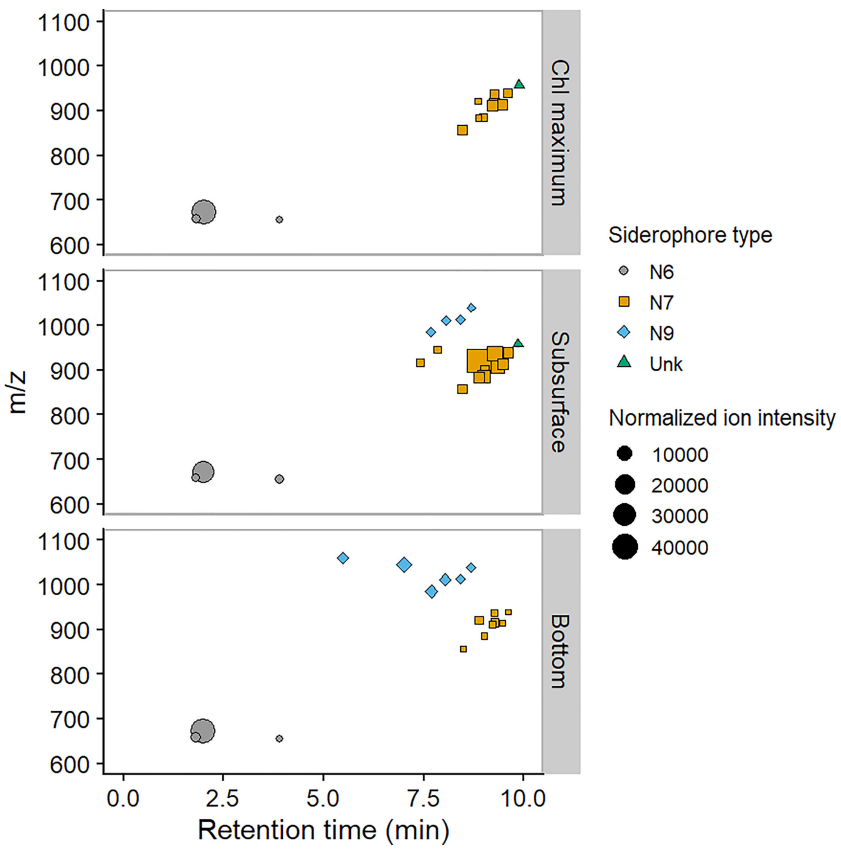


**FIGURE 2** | Plot of retention time against mass: charge (m/z) for $[M-2H+Fe]^+$ ions of siderophores identified at station CCS in November 2014. Siderophore family is shown by symbol size and colour: $N_6$ includes ferrioxamine siderophores, $N_7$ includes amphibactin siderophores and $N_9$ includes the marinobactin siderophores whilst Unk indicates siderophores where we were unable to predict molecular formulas (see **Table 1**). The size of the symbol shows ion intensities normalized to preconcentration volume.

## Siderophore Quantification – Comparison of ICP-MS and ESI-MS Detection

Whilst detection of siderophores in marine samples has been undertaken by both ESI-MS and ICP-MS, a quantitative comparison between the two approaches has yet to be made (Mawji et al., 2011; Boiteau et al., 2016; Bundy et al., 2018; Boiteau et al., 2019). We matched 11 out of 13 peaks appearing in iron ICP-MS chromatograms with those identified by ESI-MS (**Figure 3**), although overall a lower number of siderophore peaks were observed in iron ICP-MS chromatograms (12) when compared to those detected in the same chromatographic run by ESI-MS (**Table 1**), likely because of peak co-elution and the difference in detector sensitivity. We observed a good correlation between our ESI-MS and ICP-MS responses for ferrioxamines ($r^2$ = 0.99, n=52, **Figure S2**), which were present in nearly all samples. Linear relationships between ICP-MS and ESI-MS peak area showed ESI-MS responses for $N_6$, $N_7$ and $N_9$ siderophores were an estimated 36.8 ± 0.6 (n=52), 8.1 ± 0.9 (n=8) and 3.9 ± 0.7 (n=12) times the ion counts observed for corresponding ICP-MS responses (**Figure S2**). The different sensitivities observed on ESI-MS analysis are likely related to the structural differences between the siderophores (Oss et al., 2010) with $N_9$ siderophores ionising less efficiently than the $N_6$ siderophores. We also noted that some $N_7$ and $N_9$ peaks eluted at very similar retention times (e.g. $N_7$ 863.48 eluted with a similar retention time as marinobactin A; **Figure 2**), thus analysis with ICP-MS detection alone, which relies on identification by retention time, would not have been able to distinguish these two compounds using the chromatographic conditions applied in this study.

All but two of the iron peaks (peak A and K, **Figure 3**) could be allocated to an ESI-MS mass. Inability to identify siderophores corresponding to identified iron peaks could have been due to co-elution with other highly abundant ions which can result in suppression of the ESI-MS signal, or because the gallium exchange method did not work for these iron compounds. For example, we cannot detect gallium complexes of enterobactin with our method (results not shown). Our experiments therefore highlighted the utility of simultaneous ICP-MS and ESI-MS detection for the analysis of siderophores in the environment.

## Siderophore Diversity and Abundance in Northwest European Shelf Sea Waters

The water column of the Celtic Sea is seasonally stratified. At the start of our spring sampling campaign the water column was fully mixed and stratified over the course of the spring 2015 cruise (**Figure 1**). In the summer and autumn, the surface mixed layer (SML) was separated from deeper waters by a pronounced density gradient. We determined siderophore diversity and abundance in the three depth horizons (**Figure S1** and **Figures 4**, **5**) - the chlorophyll maximum (42-66 m), sub surface (below the chlorophyll maximum and surface mixed layer; 61-84 m) and close to the bottom (within 6 m of the seafloor). We discuss siderophore diversity and abundance in spring and summer first and seperately from autumn, since preconcentration was undertaken at different temperatures and this may have led to systematic bias in our results.

In spring and summer no marked trends in total siderophore concentrations with depth were observed (**Figure 4**). The mean

**TABLE 1** | Masses ($[M+^{56}Fe+H]^+$) of siderophores identified in shelf waters of the Celtic Sea.

| Mass: charge $[M-2H+^{56}Fe]^+$ | Monoisotopic mass | Retention time[a] | Predicted Formula | Delta ppm | Family | Identity |
|---|---|---|---|---|---|---|
| 640.2522 | 586.33 | 2.9 | $C_{26}H_{43}FeN_6O_9$ | 1.3 | $N_6$ | Ferrioxamine D2 |
| 654.2669 | 600.35 | 3.8 | $C_{27}H_{45}FeN_6O_9$ | 2.8 | $N_6$ | Ferrioxamine E |
| 658.2619 | 604.34 | 1.6 | $C_{26}H_{45}FeN_6O_{10}$ | 0.05 | $N_6$ | Ferrioxamine G2 |
| 672.2779 | 618.36 | 2.0 | $C_{27}H_{47}FeN_6O_{10}$ | 0.5 | $N_6$ | Ferrioxamine G |
| 857.3846 | 803.46 | 8.6 | $C_{36}H_{62}FeN_7O_{13}$ | 2.1 | $N_7$ | Amphibactin T |
| 883.4004 | 829.48 | 8.9 | $C_{38}H_{64}FeN_7O_{13}$ | 2.2 | $N_7$ | Amphibactin S |
| 885.4156 | 831.49 | 9 | $C_{38}H_{66}FeN_7O_{13}$ | 1.7 | $N_7$ | Amphibactin D |
| 901.411 | 847.49 | 9.4 | $C_{38}H_{66}FeN_7O_{14}$ | 2.2 | $N_7$ | Amphibactin B |
| 911.4298 | 857.51 | 9.2 | $C_{40}H_{68}FeN_7O_{13}$ | 0.08 | $N_7$ | Amphibactin E |
| 913.4473 | 859.52 | 9.6 | $C_{40}H_{70}FeN_7O_{13}$ | 2.1 | $N_7$ | Amphibactin H |
| 915.4265 | 861.50 | 9.3 | $C_{39}H_{68}FeN_7O_{14}$ | 2.0 | $N_7$ | |
| 917.4022 | 863.48 | 7.4 | $C_{38}H_{66}FeN_7O_{15}$ | 1.9 | $N_7$ | |
| 921.4141 | 867.50 | 8.9 | $C_{41}H_{66}FeN_7O_{13}$ | 0.02 | $N_7$ | |
| 937.4089 | 883.49 | 9.4 | $C_{41}H_{66}FeN_7O_{14}$ | 0.1 | $N_7$ | |
| 939.4608 | 885.54 | 9.6 | $C_{42}H_{72}FeN_7O_{13}$ | 0.2 | $N_7$ | Amphibactin I |
| 945.4350 | 891.52 | 8.3 | $C_{40}H_{70}FeN_7O_{15}$ | 0.2 | $N_7$ | |
| 957.375 | 903.46 | 6.8 | $C_{38}H_{62}FeN_9O_{16}$ | 0.1 | $N_9$ | |
| 958.505 | 904.59 | 9.8 | | | Unassigned | |
| 985.4035 | 931.49 | 7.7 | $C_{40}H_{66}FeN_9O_{16}$ | 1.5 | $N_9$ | Marinobactin A |
| 1011.42 | 957.50 | 8 | $C_{42}H_{68}FeN_9O_{16}$ | 0.6 | $N_9$ | Marinobactin B |
| 1013.435 | 959.52 | 8.4 | $C_{42}H_{70}FeN_9O_{16}$ | 1.3 | $N_9$ | Marinobactin C |
| 1039.454 | 987.54 | 8.6 | $C_{44}H_{72}FeN_9O_{16}$ | 2 | $N_9$ | Marinobactin E |
| 1045.424 | 991.51 | 7 | $C_{42}H_{70}FeN_9O_{18}$ | 2 | $N_9$ | |
| 1059.405 | 1005.49 | 5.6 | $C_{42}H_{68}FeN_9O_{19}$ | 0.3 | $N_9$ | |

[a]*Determined for analysis (1) and (2) as described in the methods.*

*Also provided are the monoisotopic mass for the iron free form of the siderophore, the retention times using conditions applied for siderophore identification, predicted formulas together with the difference in mass between the observed and predicted $[M-2H+^{56}Fe]^+$ ion and, where possible the assigned identity.*

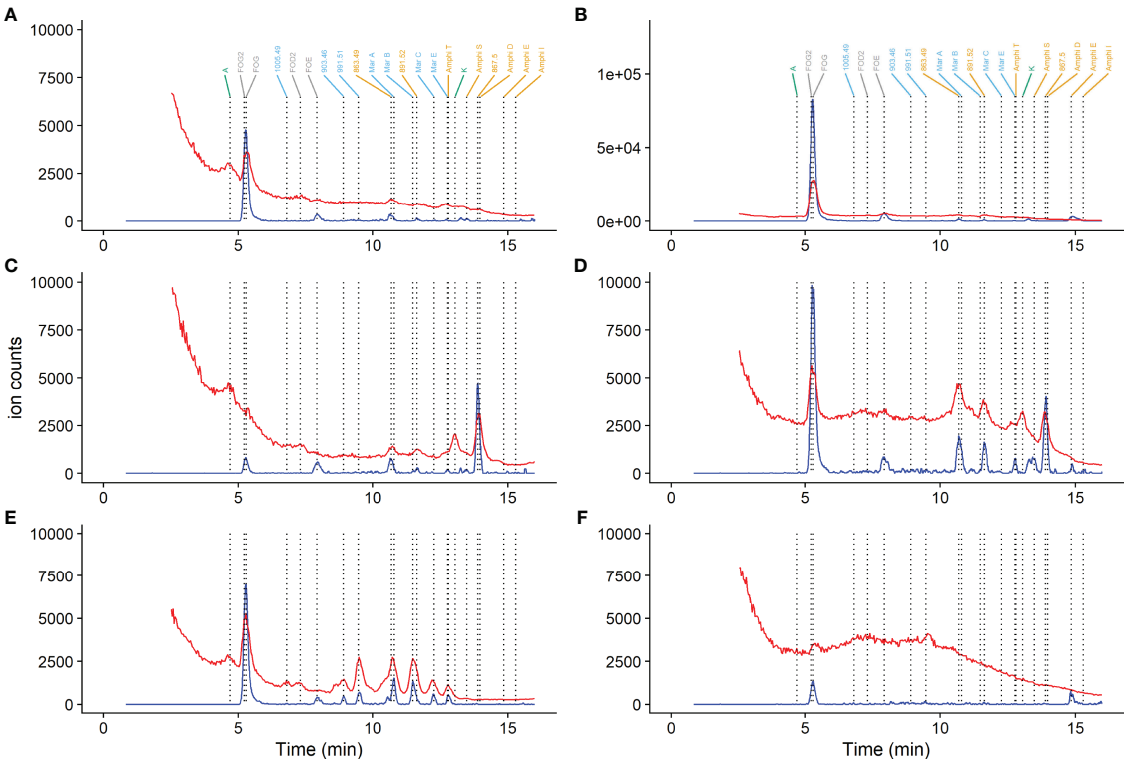


**FIGURE 3** | Example chromatograms obtained in November 2014 from CCS **(A, C, E)** and CS2 **(B, D, F)** for the chlorophyll maximum **(A, B)**, subsurface samples **(C, D)** and bottom depths **(E, F)**. The red line is for the abundance of $^{56}Fe$ obtained by ICP-MS and the blue line the extracted ion chromatogram for the sum of all $[M\text{-}2H+Fe]^+$ ions given in **Table 1**. Ion intensity was normalised relative to extraction volume. Ions are coloured according to siderophore group, with $N_6$ siderophores indicated in grey text, $N_7$ in orange text, $N_9$ in blue text and unknown in green text. The key to peak labels is given in **Supplementary Table 2**.

total siderophore concentration observed at CCS in April was 4.9 ± 1.1 pmol $L^{-1}$ (n=3) and in July was 3.8 ± 2.8 pmol $L^{-1}$ (n=6; **Figure 4**). We observed up to five different siderophores in our spring and summer samples (**Figure 5**). Ferrixoamine ($N_6$) siderophores were ubiquitous, and in spring and summer we detected FOG in all but one sample (**Figure 5**). Ferrioxamine G was the dominant siderophore in summer, but in spring, most of the Fe was associated with peak A, an unidentified compound we did

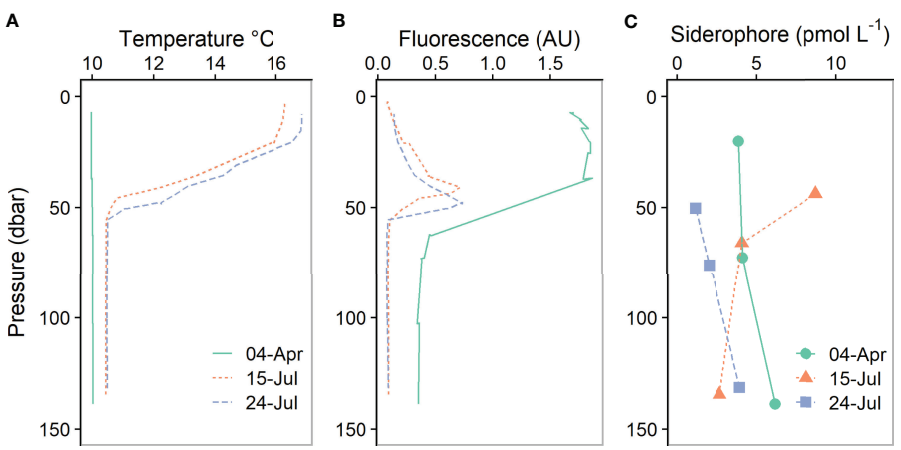


**FIGURE 4** | Depth profiles showing **(A)** temperature, **(B)** fluorescence and **(C)** total siderophore concentrations observed in spring (April 2015) and summer (July 2015).

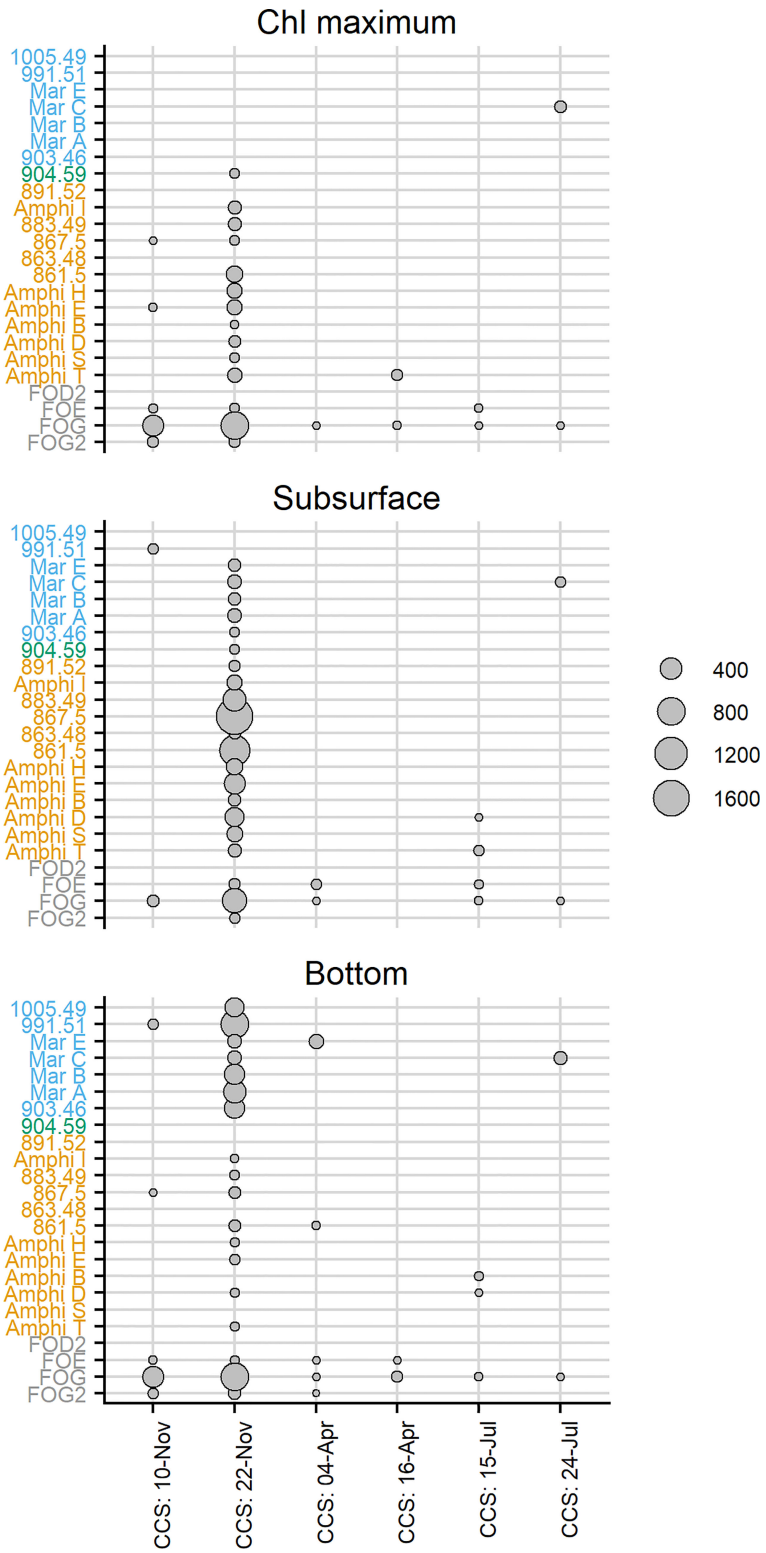


**FIGURE 5** | Bubble plot showing normalised ion intensities for each siderophore at the chlorophyll maximum (upper panel), subsurface (middle panel) and at the bottom of the water column (lower panel). Ion intensities were normalised for preconcentration volume and as a function of ESI-MS ionisation efficiency using the response for the $[M\text{-}2H+Fe]^+$ obtained on detection by ESI-MS, relative to the $^{56}Fe$ obtained using ICP-MS. The axis text colour indicates the siderophore families identified in the samples, with $N_6$ siderophores indicated in grey text, $N_7$ in orange text, $N_9$ in blue text and unknown in green text.

not detect a corresponding peak for using ESI-MS (**Figure 3**). In addition to ferrioxamines and peak A, trace levels of $N_7$ (Amphibactins T, S, D and B) and $N_9$ siderophores (Marinobactin A and C), were observed sporadically. However none of these siderophores were present at concentrations high enough to be detected by ICP-MS in spring or summer.

In autumn (November 2014), total siderophore concentrations and siderophore diversity on one profile from CS2 and on one profile at CCS, were considerably higher than those observed in spring and summer (**Figure S2**). The high concentrations of siderophores in these samples facilitated confident identification of compounds in Ga exchange experiments, but it is difficult to be certain that the observed concentrations were not the result of bacterial production of siderophores during preconcentration of the sample. Preconcentration took ca. four days and was undertaken at approximately 20°C (in spring and summer cruises, preconcentration was carried out at 4°C), conditions which are potentially favourable for growth of copiotrophic bacteria, which are likely responsible for siderophore production (Vraspir and Butler, 2009). We suggest that although concentrations could be biased, variations in the occurrence of individual siderophores likely reflect potential for siderophore production in the ambient bacterial population. In this regard, we note a trend in the occurrence of the different groups of siderophores with depth. Ferrioxamines ($N_6$) were the dominant siderophore at the chlorophyll maximum in November, whilst $N_7$ siderophores were more abundant in subsurface samples, and $N_9$ siderophores were more abundant in bottom waters (**Figure 5**). Taken together with previous reports on the distributions of siderophores, our work supports suggestions that production of siderophores could be highly dynamic although $N_6$ siderophores appear to be somewhat ubiqitous (Mawji et al., 2008; Boiteau et al., 2016; Velasquez et al., 2016; Bundy et al., 2018). We also note that marinobactins are mixed α-hydroxy carboxylate siderophores and, when complexed to iron, have greater sensitivity to photochemical degradation than hydroxamate type siderophores (Barbeau et al., 2003). Thus, it was notable that $N_9$ siderophores were most abundant below the photic zone, as recently observed for petrobactins, another photosenstive type of siderophore (Manck et al., 2021). We suggest that the bacterial species responsible for $N_9$ production may be more abundant in sub photic zone environments, where photochemical breakdown of siderophores would not occur. The proximity of our bottom sample to the sediment also highlights a potential sedimentary source for $N_9$ siderophores.

## Impact of Siderophores on Dissolved Iron Speciation in the Water Column

The siderophores we detected in our samples are one component of a complex mix of inorganic and organic counter ions and binding sites that are present in seawater (Gledhill and Buck, 2012). DOM comprises a heterogeneous mixture of an estimated $10^5$ different molecules, likely present at individual concentrations of < 10 pmol $L^{-1}$ (Zark et al., 2017). Siderophores compete for iron with hydroxide ions and with other binding sites in DOM, which have been shown to have humic-like binding characteristics (Laglera et al., 2019; Lodeiro et al., 2020; Whitby et al., 2020; Fourrier et al., 2021; Zhu et al., 2021a). Although the majority of these binding sites will not have a high enough affinity for iron to compete with the hydroxide ion, a small portion have structures that facilitate metal binding and a further fraction of these ions may be sufficiently strong enough to compete with siderophores, particularly when dissolved iron concentrations are low (Gledhill and Gerringa, 2017; Lodeiro et al., 2020). Binding site heterogeneity also means that the relative distribution of iron between the different competing groups (i.e., siderophores and humic substance-like binding sites in DOM) will not remain constant as iron concentrations change (Gledhill and Gerringa, 2017). Here, we use a combined ion-pair NICA-Donnan model to assess competition between siderophores and humic substance-like binding sites present in DOM and calculate the distribution of iron between the different chemical groups. For iron we consider four reactions that comprise the major competitors for the free iron ion ($Fe^{3+}$): Equation (1) - iron binding to aqueous inorganic ions (Fe′), of which the most important counter ions for iron in seawater are the hydroxides (Turner et al., 1981), equation (2) - iron binding to binding sites in DOM (FeDOM), equation (3) - iron binding to siderophores (Sid), and equation (4) formation of solid iron hydroxides (which could be colloidal), as outlined in Zhu et al. (2021b, 2021a).

$$Fe^{3+} + (3-i)OH^- \leftrightarrow Fe(OH)_i^{3-i} \quad (1)$$

$$Fe^{3+} + DOM^{x-} \leftrightarrow Fe(DOM)^{3-x} \quad (2)$$

$$Fe^{3+} + Sid^{3-} \leftrightarrow FeSid \quad (3)$$

$$Fe^{3+} + 3OH^- \rightarrow Fe(OH)_3(s) \quad (4)$$

We calculated speciation at two total iron concentrations: a high iron environment (iron concentration = 1.9 nmol $L^{-1}$) and a low iron environment (iron concentration = 0.3 nmol $L^{-1}$). These concentrations are representative of the highest and lowest dissolved iron concentrations observed at CCS below the surface mixed layer and in the surface mixed layer at the times our siderophore samples were collected (Birchill et al., 2017).

We calculated the distribution of iron species as a function of siderophore concentration (**Figure 6**). As expected, the proportion of FeSid increases with increasing siderophore concentrations, however as siderophore concentrations approach the iron concentration, the increase becomes non-linear. In the high iron scenario, where calculated $Fe^{3+}$ concentrations exceed its solubility limit (Zhu et al., 2021a), increasing siderophore concentrations do not impact on Fe′ or FeDOM until the siderophore concentration is in excess of Fe $(OH)_3(s)$, which in our scenario equated to a total siderophore concentration close to 1 nmol $L^{-1}$. Therefore, when $Fe^{3+}$ is oversaturated with respect to $Fe(OH)_3(s)$, siderophore production first prevents the formation of $Fe(OH)_3(s)$. At concentrations of total siderophore below 1 nmol $L^{-1}$, we

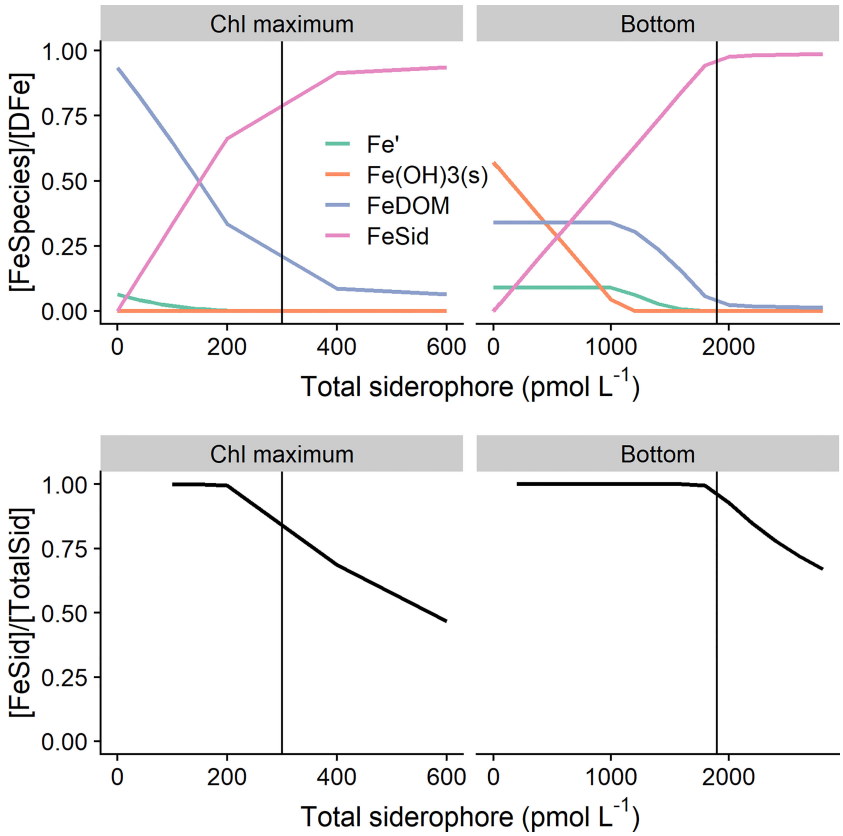


**FIGURE 6** | Calculated species distributions for 0.3 (left panels) and 1.9 nmol $L^{-1}$ (right panels) iron concentration expressed as the concentration of the species ([FeSpecies]) divided by the concentration of iron ([Fe]). Iron concentrations (pmol $L^{-1}$) are indicated by the vertical black line and were representative of dissolved iron concentrations observed in the chlorophyll maximum (Chl maximum) and close to the sediment (Bottom) respectively. Top panels show the abundance of inorganic Fe (Fe′), Fe bound to dissolved organic matter (FeDOM), Fe bound to siderophores (FeSid) and Fe present as ($Fe(OH)_3$(s) relative to the total iron concentration as a function of increasing total siderophore concentration. Bottom panels show the proportion of iron bound to siderophores relative to the total siderophore concentration as a function of increasing total siderophore concentration.

calculate a constant Fe′ concentration of 170 pmol $L^{-1}$, since Fe′ is determined directly by the saturation concentration of $Fe^{3+}$ at the applied pH and temperature (Zhu et al., 2021a). However, we highlight that the highest siderophore concentrations observed in our study below the SML were well below 1 nmol $L^{-1}$ (**Figure 4**). The calculated FeSid concentrations would thus be close to or lower than both Fe′ and FeDOM below the SML at stations CCS and CS2. Our calculations are therefore in contrast to previous calculations based on conditional stability constants, where FeSid was determined to be higher than Fe′, but the heterogeneity of DOM binding sites was not considered (Bundy et al., 2018). In the low iron scenario, $Fe^{3+}$ concentrations were undersaturated, so formation of $Fe(OH)_3$(s) was not predicted in our calculations. Consequently, increasing siderophore concentrations resulted in reduced Fe′ and FeDOM. However, FeSid did not become the dominant species until the total siderophore concentration was 50% of the total dissolved iron concentration, and even when the total siderophore concentration is equal to the total dissolved iron concentration then approximately 25% of DFe was calculated as bound to the humic substance-like binding sites in DOM. These calculations are thus consistent with the apparent undersaturation of siderophores isolated from seawater observed in other studies (Boiteau et al., 2016; Manck et al., 2021).

There is still some uncertainty in these calculations relating to the parameters chosen to describe FeDOM and the degree of DOM heterogeneity, strongly influences the relationship between Fe′ and total dissolved iron concentrations (Zhu et al., 2021a; Zhu et al., 2021b). In particular, the degree of heterogeneity as represented by the non-ideality constant ($n$) has been shown to be quite variable (Lodeiro et al., 2021; Zhu et al., 2021a; Zhu et al., 2021b). Furthermore, parameters derived for the phenolic-like binding sites in marine DOM appear to be subject to some uncertainty and variability, likely because phenolic-like binding sites are relatively less abundant in marine DOM and thus harder to constrain in both proton and iron titration experiments (Lodeiro et al., 2021; Zhu et al., 2021b). Nevertheless, our results suggest that at low DFe concentrations, high affinity binding sites in the heterogeneous DOM pool could be effective competitors for siderophores. An

important consequence of this is that it would be very difficult to distinguish siderophores from humic substance-like binding sites present in marine DOM by titration techniques typically applied to investigate iron speciation in seawater (Gledhill and van den Berg, 1994; Croot and Johansson, 2000; Buck et al., 2007; Gerringa et al., 2021). The often used categorisation into ligand groups based on conditional stability constants is thus not as well defined as previously suggested (Gledhill and Buck, 2012).

## CONCLUSIONS

Our results add to the growing evidence that siderophore production occurs widely in the marine environment and many marine bacteria possess the ability to produce (and utilise) siderophores. Nevertheless the impact of siderophore production on iron biogeochemistry is not straightforward. The heterogeneous distribution of binding sites in the humic-like component of marine DOM means that a proportion of the humic-like binding sites could be effective competitors with siderophores. The binding of iron to siderophores is thus likely to be influenced by the distribution of binding site strengths (i.e. intrinsic heterogeneity) of the humic substance-like component of marine DOM and the dissolved iron concentration and attribution of different conditional binding site strengths (i.e. conditional stability constants) to the presence of different types of compounds should therefore be avoided. Considering siderophores are often cited as being an iron acquisition strategy designed to increase iron availability to the producer, our prediction that the siderophore concentrations we observed at depth could be lower than Fe′ is surprising given Fe′ is considered the most bioavailable form of iron (Shaked and Lis, 2012). It should be born in mind that our findings are influenced by both the binding parameters used in the NICA model, and the thermodynamic constants used to describe the siderophore pool and further derivations of both NICA parameters and thermodynamic constants for marine siderophores would therefore be useful and further constrain the resultant speciation calculations. Nevertheless, if we further consider the energetic cost of siderophore production and the likelyhood of siderophore retrieval by producers (Völker and Wolf-Gladrow, 1999; Niehus et al., 2017), our results could point towards a key role for microenvironments such as gels, biofilms or particles where conditions maybe more favourable for siderophore production and retrieval than in the bulk seawater examined in our study. Further studies that combine investigations of siderophore abundance with determination of iron speciation in a way that fully accounts for DOM binding site heterogeneity and ambient physico-chemical conditions are therefore required to unravel the complex drivers that likely influence the abundance and diversity of siderophores in the ocean and their impact on iron biogeochemistry.

## DATA AVAILABILITY STATEMENT

The original contributions presented in the study are included in the article/**Supplementary Material**. Further inquiries can be directed to the corresponding author.

## AUTHOR CONTRIBUTIONS

MG designed the study, performed the analysis. KZ carried out the NICA-Donnan modelling. DR contributed to study design and collected the samples. EA designed the study. MG, KZ, DR, and EA all contributed to the manuscript. All authors contributed to the article and approved the submitted version.

## FUNDING

The project was funded by the UK Natural Environment Research Council, NE/K001973/1 (EA and MG) and the Helmholtz Association. KZ was supported by a scholarship from the China Scholarship Council.

## ACKNOWLEDGMENTS

We thank the captain and crew of the RSS Discovery. We thank C. Schlosser for his assistance with the ICP-MS analysis. The authors declare no competing financial interest.

## SUPPLEMENTARY MATERIAL

The Supplementary Material for this article can be found online at: https://www.frontiersin.org/articles/10.3389/fmars.2022.855009/full#supplementary-material

## REFERENCES

Baars, O., Morel, F. M. M., and Perlman, D. H. (2014). ChelomEx: Isotope-Assisted Discovery of Metal Chelates in Complex Media Using High-Resolution LC-MS. *Anal. Chem.* 86, 11298–11305. doi: 10.1021/ac503000e

Barbeau, K., Rue, E. L., Trick, C. G., Bruland, K. T., and Butler, A. (2003). Photochemical Reactivity of Siderophores Produced by Marine Heterotrophic Bacteria and Cyanobacteria Based on Characteristic Fe (III) Binding Groups. *Limnol. Oceanogr.* 48, 1069–1078. doi: 10.4319/lo.2003.48.3.1069

Birchill, A. J., Milne, A., Woodward, E. M. S., Harris, C., Annett, A., Rusiecka, D., et al (2017). Seasonal Iron Depletion in Temperate Shelf Seas. *Geophys. Res. Lett.* 44, 8987–8996. doi: 10.1002/2017GL073881

Boiteau, R. M., Fitzsimmons, J. N., Repeta, D. J., and Boyle, E. A. (2013). Detection of Iron Ligands in Seawater and Marine Cyanobacteria Cultures by High-Performance Liquid Chromatography–Inductively Coupled Plasma-Mass Spectrometry. *Anal. Chem.* 85, 4357–4362. doi: 10.1021/ac3034568

Boiteau, R. M., Mende, D. R., Hawco, N. J., McIlvin, M. R., Fitzsimmons, J. N., Saito, M. A., et al (2016). Siderophore-Based Microbial Adaptations to Iron Scarcity Across the Eastern Pacific Ocean. *Proc. Natl. Acad. Sci. U.S.A.* 113, 14237–14242. doi: 10.1073/pnas.1608594113

Boiteau, R. M., Till, C. P., Coale, T. H., Fitzsimmons, J. N., Bruland, K. W., and Repeta, D. J. (2019). Patterns of Iron and Siderophore Distributions Across the California Current System. *Limnol. Oceanogr.* 64, 376–389. doi: 10.1002/lno.11046

Boyd, P. W., and Ellwood, M. J. (2010). The Biogeochemical Cycle of Iron in the Ocean. *Nat. Geosci.* 3, 675–682. doi: 10.1038/ngeo964

Buck, K. N., Lohan, M. C., Berger, C. J. M., and Bruland, K. W. (2007). Dissolved Iron Speciation in Two Distinct River Plumes and an Estuary: Implications for Riverine Iron Supply. *Limnol. Oceanogr.* 52, 843–855. doi: 10.4319/lo.2007.52.2.0843

Buck, K. N., Sedwick, P. N., Sohst, B., and Carlson, C. A. (2018). Organic Complexation of Iron in the Eastern Tropical South Pacific: Results From US GEOTRACES Eastern Pacific Zonal Transect (GEOTRACES Cruise GP16). *Mar. Chem.* 201, 229–241. doi: 10.1016/J.MARCHEM.2017.11.007

Bundy, R. M., Biller, D. V., Buck, K. N., Bruland, K. W., and Barbeau, K. A. (2014). Distinct Pools of Dissolved Iron-Binding Ligands in the Surface and Benthic Boundary Layer of the California Current. *Limnol. Oceanogr.* 59, 769–787. doi: 10.4319/lo.2014.59.3.0769

Bundy, R. M., Boiteau, R. M., McLean, C., Turk-Kubo, K. A., McIlvin, M. R., Saito, M. A., et al (2018). Distinct Siderophores Contribute to Iron Cycling in the Mesopelagic at Station ALOHA. *Front. Mar. Sci.* 5. doi: 10.3389/fmars.2018.00061

Croot, P. L., and Johansson, M. (2000). Determination of Iron Speciation by Cathodic Stripping Voltammetry in Seawater Using the Competing Ligand 2-(2-Thiazolylazo)-P-Cresol (TAC). *Electoanalysis* 12, 565–576. doi: 10.1002/(SICI)1521-4109(200005)12:8<565::AID-ELAN565>3.0.CO;2-L

Davis, C. E., Blackbird, S., Wolff, G., Woodward, M., and Mahaffey, C. (2018). Seasonal Organic Matter Dynamics in a Temperate Shelf Sea. *Prog. Oceanogr.* 177, 101925. doi: 10.1016/J.POCEAN.2018.02.021

Fourrier, P., Dulaquais, G., Guigue, C., Giamarchi, P., Sarthou, G., Whitby, H., et al (2021). Characterization of the Vertical Size Distribution, Composition and Chemical Properties of Dissolved Organic Matter in the (Ultra) Oligotrophic Pacific Ocean Through a Multi-Detection Approach. *Mar. Chem.* 240, 104068. doi: 10.1016/J.MARCHEM.2021.104068

Fraústo Da Silva, J. J. R. (1983). The Chelate Effect Redefined. *J. Chem. Educ.* 60, 390–392. doi: 10.1021/ED060P390

Gerringa, L. J. A., Gledhill, M., Ardiningsih, I., Muntjewerf, N., and Laglera, L. M. (2021). Comparing CLE-AdCSV Applications Using SA and TAC to Determine the Fe-Binding Characteristics of Model Ligands in Seawater. *Biogeosciences* 18, 5265–5289. doi: 10.5194/BG-18-5265-2021

Gledhill, M., Basu, S., and Shaked, Y. (2019). Metallophores Associated With *Trichodesmium Erythraeum* Colonies From the Gulf of Aqaba. *Metallomics* 11, 1547–1557. doi: 10.1039/C9MT00121B

Gledhill, M., and Buck, K. N. (2012). The Organic Complexation of Iron in the Marine Environment: A Review. *Front. Microbiol.* 3. doi: 10.3389/fmicb.2012.00069

Gledhill, M., and Gerringa, L. J. A. (2017). The Effect of Metal Concentration on the Parameters Derived From Complexometric Titrations of Trace Elements in Seawater—A Model Study. *Front. Mar. Sci.* 4. doi: 10.3389/fmars.2017.00254

Gledhill, M., McCormack, P., Ussher, S., Achterberg, E. P., Mantoura, R. F. C., and Worsfold, P. J. (2004). Production of Siderophore Type Chelates by Mixed Bacterioplankton Populations in Nutrient Enriched Seawater Incubations. *Mar. Chem.* 88, 75–83. doi: 10.1016/j.marchem.2004.03.003

Gledhill, M., and van den Berg, C. M. G. (1994). Determination of Complexation of Iron(III) With Natural Organic Complexing Ligands in Seawater Using Cathodic Stripping Voltammetry. *Mar. Chem.* 47, 41–54. doi: 10.1016/0304-4203(94)90012-4

Hider, R. C., and Kong, X. L. (2010). Chemistry and Biology of Siderophores. *Natural Prod. Rep.* 27, 637–657. doi: 10.1039/b906679a

Hiemstra, T., and van Riemsdijk, W. H. (2006). Biogeochemical Speciation of Fe in Ocean Water. *Mar. Chem.* 102, 181–197. doi: 10.1016/j.marchem.2006.03.008

Hogle, S. L., Hackl, T., Bundy, R. M., Park, J., Satinsky, B., Satinsky, B., et al (2021). Siderophores as an Iron Source for Prochlorococcus in Deep Chlorophyll Maximum Layers of the Oligotrophic Ocean. *bioRxiv*, 2021.11.13.468467. doi: 10.1101/2021.11.13.468467

Hutchins, D. A., and Boyd, P. W. (2016). Marine Phytoplankton and the Changing Ocean Iron Cycle. *Nat. Climate Change* 6, 1072–1079. doi: 10.1038/nclimate3147

Kind, T., and Fiehn, O. (2007). Seven Golden Rules for Heuristic Filtering of Molecular Formulas Obtained by Accurate Mass Spectrometry. *BMC Bioinform.* 8, 105. doi: 10.1186/1471-2105-8-105

Kinniburgh, D. G., Milne, C. J., Benedeti, M. F., Pinheiro, J. P., Filius, J., Koopal, L. K., et al (1996). Metal Ion Binding by Humic Acid: Application of the NICA-Donnan Model. *Environ. Sci. Technol.* 30, 1687–1698. doi: 10.1021/es950695h

Laglera, L. M., Battaglia, G., and van den Berg, C. M. G. (2007). Determination of Humic Substances in Natural Waters by Cathodic Stripping Voltammetry of Their Complexes With Iron. *Anal. Chim. Acta* 599, 58–66. doi: 10.1016/j.aca.2007.07.059

Laglera, L. M., Sukekava, C., Slagter, H. A., Downes, J., Aparicio-Gonzalez, A., and Gerringa, L. J. A. (2019). First Quantification of the Controlling Role of Humic Substances in the Transport of Iron Across the Surface of the Arctic Ocean. *Environ. Sci. Technol.* 53, 13136–13145. doi: 10.1021/ACS.EST.9B04240

Lee, W., van Baalen, M., and Jansen, V. A. A. (2012). An Evolutionary Mechanism for Diversity in Siderophore-Producing Bacteria. *Ecol. Lett.* 15, 119–125. doi: 10.1111/j.1461-0248.2011.01717.x

Liu, X., and Millero, F. J. (1999). The Solubility of Iron Hydroxide in Sodium Chloride Solutions. *Geochim. Cosmochim. Acta* 63, 3487–3497. doi: 10.1016/S0016-7037(99)00270-7

Liu, X., and Millero, F. J. (2002). The Solubility of Iron in Seawater. *Mar. Chem.* 77, 43–54. doi: 10.1016/S0304-4203(01)00074-3

Lodeiro, P., Rey-Castro, C., David, C., Achterberg, E. P., Puy, J., and Gledhill, M. (2020). Acid-Base Properties of Dissolved Organic Matter Extracted From the Marine Environment. *Sci. Total Environ.* 729, 138437. doi: 10.1016/j.scitotenv.2020.138437

Lodeiro, P., Rey-Castro, C., David, C., Puy, J., Achterberg, E. P., and Gledhill, M. (2021). Seasonal Variations in Proton Binding Characteristics of Dissolved Organic Matter Isolated From the Southwest Baltic Sea. *Environ. Sci. Technol.* 55, 16215–16223. doi: 10.1021/ACS.EST.1C04773

Manck, L. E., Park, J., Tully, B. J., Poire, A. M., Bundy, R. M., Dupont, C. L., et al (2021). Petrobactin, a Siderophore Produced by Alteromonas, Mediates Community Iron Acquisition in the Global Ocean. *ISME J.* 2021, 1–12. doi: 10.1038/s41396-021-01065-y

Martinez, J. S., and Butler, A. (2007). Marine Amphiphilic Siderophores: Marinobactin Structure, Uptake, and Microbial Partitioning. *J. Inorg. Biochem.* 101, 1692–1698. doi: 10.1016/j.jinorgbio.2007.07.007

Martinez, J. S., Carter-Franklin, J. N., Mann, E. L., Martin, J. D., Haygood, M. G., and Butler, A. (2003). Structure and Membrane Affinity of a Suite of Amphiphilic Siderophores Produced by a Marine Bacterium. *Proc. Natl. Acad. Sci. U.S.A.* 100, 3754–3759. doi: 10.1073/pnas.0637444100

Martinez, J. S., Zhang, G. P., Holt, P. D., Jung, H.-T., Carrano, C. J., Haygood, M. G., et al (2000). Self-Assembling Amphiphilic Siderophores From Marine Bacteria. *Science* 287, 1245–1247. doi: 10.1126/science.287.5456.1245

Mawji, E., Gledhill, M., Milton, J. A., Tarran, G. A., Ussher, S., Thompson, A., et al (2008). Hydroxamate Siderophores: Occurrence and Importance in the Atlantic Ocean. *Environ. Sci. Technol.* 42, 8675–8680. doi: 10.1021/es801884r

Mawji, E., Gledhill, M., Milton, J. A., Zubkov, M. V., Thompson, A., Wolff, G. A., et al (2011). Production of Siderophore Type Chelates in Atlantic Ocean Waters Enriched With Different Carbon and Nitrogen Sources. *Mar. Chem.* 124, 90–99. doi: 10.1016/j.marchem.2010.12.005

McCormack, P., Worsfold, P. J., and Gledhill, M. (2003). Separation and Detection of Siderophores Produced by Marine Bacterioplankton Using High-Performance Liquid Chromatography With Electrospray Ionization Mass Spectrometry. *Anal. Chem.* 75, 2647–2652. doi: 10.1021/ac0340105

Meeussen, J. C. L. (2003). Orchestra: An Object-Oriented Framework for Implementing Chemical Equilibrium Models. *Environ. Sci. Technol.* 37, 1175–1182. doi: 10.1021/es025597s

Milne, C. J., Kinniburgh, D. G., and Tipping, E. (2001). Generic NICA-Donnan Model Parameters for Proton Binding by Humic Substances. *Environ. Sci. Technol.* 35, 2049–2059. doi: 10.1021/es000123j

Milne, C. J., Kinniburgh, D. G., van Riemsdijk, W. H., and Tipping, E. (2003). Generic NICA–Donnan Model Parameters for Metal-Ion Binding by Humic Substances. *Environ. Sci. Technol.* 37, 958–971. doi: 10.1021/es0258879

Niehus, R., Picot, A., Oliveira, N. M., Mitri, S., and Foster, K. R. (2017). The Evolution of Siderophore Production as a Competitive Trait. *Evolution* 71, 1443–1455. doi: 10.1111/EVO.13230

Oss, M., Kruve, A., Herodes, K., and Leito, I. (2010). Electrospray Ionization Efficiency Scale of Organic Compounds. *Anal. Chem.* 82, 2865–2872. doi: 10.1021/AC902856T

Perdue, E. M., and Lytle, C. R. (1983). Distribution Model for Binding of Protons and Metal Ions by Humic Substances. *Environ. Sci. Technol.* 17, 654–660. doi: 10.1021/es00117a006

Pluskal, T., Castillo, S., Villar-Briones, A., and Orešič, M. (2010). MZmine 2: Modular Framework for Processing, Visualizing, and Analyzing Mass Spectrometry-Based Molecular Profile Data. *BMC Bioinform.* 11, 1–11. doi: 10.1186/1471-2105-11-395

Poulton, A. J., Davis, C. E., Daniels, C. J., Mayers, K. M. J., Harris, C., Tarran, G. A., et al (2017). Seasonal Phosphorus and Carbon Dynamics in a Temperate Shelf Sea (Celtic Sea). *Prog. Oceanogr.* 177, 101872. doi: 10.1016/J.POCEAN.2017.11.001

R Development Core Team (2016). *R: A Language and Environment for Statistical Computing* (Vienna Austria: R Foundation for Statistical Computing), ISBN: . doi: 10.1038/sj.hdy.6800737

Ronan, J. L., Kadi, N., McMahon, S. A., Naismith, J. H., Alkhalaf, L. M., and Challis, G. L. (2018). Desferrioxamine Biosynthesis: Diverse Hydroxamate Assembly by Substrate-Tolerant Acyl Transferase DesC. *Philos. Trans. R. Soc. B: Biol. Sci.* 373, 20170068. doi: 10.1098/RSTB.2017.0068

Rusiecka, D., Gledhill, M., Milne, A., Achterberg, E. P., Annett, A. L., Atkinson, S., et al (2018). Anthropogenic Signatures of Lead in the Northeast Atlantic. *Geophys. Res. Lett.* 45, 2734–2743. doi: 10.1002/2017GL076825

Sañudo-Wilhelmy, S. A., Cutter, L. S., Durazo, R., Smail, E. A., Gómez-Consarnau, L., Webb, E. A., et al (2012). Multiple B-Vitamin Depletion in Large Areas of the Coastal Ocean. *Proc. Natl. Acad. Sci. U.S.A.* 109, 14041–14045. doi: 10.1073/pnas.1208755109

Schijf, J., and Burns, S. M. (2016). Determination of the Side-Reaction Coefficient of Desferrioxamine B in Trace-Metal-Free Seawater. *Front. Mar. Sci.* 3. doi: 10.3389/fmars.2016.00117

Shaked, Y., and Lis, H. (2012). Disassembling Iron Availability to Phytoplankton. *Front. Microbiol.* 3. doi: 10.3389/fmicb.2012.00123

Slagter, H. A., Reader, H. E., Rijkenberg, M. J. A., Rutgers van der Loeff, M., de Baar, H. J. W., and Gerringa, L. J. A. (2017). Organic Fe Speciation in the Eurasian Basins of the Arctic Ocean and its Relation to Terrestrial DOM. *Mar. Chem.* 197, 11–25. doi: 10.1016/j.marchem.2017.10.005

Tipping, E. (1993). Modeling the Competition Between Alkaline Earth Cations and Trace Metal Species for Binding by Humic Substances. *Environ. Sci. Technol.* 27, 520–529. doi: 10.1021/es00040a011

Tipping, E., Lofts, S., and Sonke, J. E. (2011). Humic Ion-Binding Model VII: A Revised Parameterisation of Cation-Binding by Humic Substances. *Environ. Chem.* 8, 225–235. doi: 10.1071/EN11016

Turner, D. R., Whitfield, M., and Dickson, A. G. (1981). The Equilibrium Speciation of Dissolved Components in Freswater and Seawater at 25°C at 1 Atm. Pressure. *Geochim. Cosmochim. Acta* 45, 855–882. doi: 10.1016/0016-7037(81)90115-0

Velasquez, I. B., Ibisanmi, E., Maas, E. W., Boyd, P. W., Nodder, S., and Sander, S. G. (2016). Ferrioxamine Siderophores Detected Amongst Iron Binding Ligands Produced During the Remineralization of Marine Particles. *Front. Mar. Sci.* 3. doi: 10.3389/fmars.2016.00172

Völker, C., and Wolf-Gladrow, D. A. (1999). Physical Limits on Iron Uptake Mediated by Siderophores or Surface Reductases. *Mar. Chem.* 65, 227–244. doi: 10.1016/S0304-4203(99)00004-3

Vraspir, J. M., and Butler, A. (2009). Chemistry of Marine Ligands and Siderophores. *Annu. Rev. Mar. Sci.* 1, 43–63. doi: 10.1146/annurev.marine.010908.163712

Whitby, H., Planquette, H., Cassar, N., Bucciarelli, E., Osburn, C. L., Janssen, D. J., et al (2020). A Call for Refining the Role of Humic-Like Substances in the Oceanic Iron Cycle. *Sci. Rep.* 10, 1–12. doi: 10.1038/s41598-020-62266-7

Wihsgott, J. U., Sharples, J., Hopkins, J. E., Woodward, E. M. S., Hull, T., Greenwood, N., et al (2019). Observations of Vertical Mixing in Autumn and its Effect on the Autumn Phytoplankton Bloom. *Prog. Oceanogr.* 177, 102059. doi: 10.1016/j.pocean.2019.01.001

Xu, G. F., Martinez, J. S., Groves, J. T., and Butler, A. (2002). Membrane Affinity of the Amphiphilic Marinobactin Siderophores. *J. Am. Chem. Soc.* 124, 13408–13415. doi: 10.1021/ja026768w

Zark, M., Christoffers, J., and Dittmar, T. (2017). Molecular Properties of Deep-Sea Dissolved Organic Matter are Predictable by the Central Limit Theorem: Evidence From Tandem FT-ICR-MS. *Mar. Chem.* 191, 9–15. doi: 10.1016/J.MARCHEM.2017.02.005

Zhu, K., Birchill, A. J., Milne, A., Ussher, S. J., Humphreys, M. P., Carr, N., et al (2021a). Equilbrium Calculations of Iron Speciation and Apparent Iron Solubility in the Celtic Sea at Ambient pH Using the NICA-Donnan Model. *Mar. Chem.* 237, 104038. doi: 10.1016/j.marchem.2021.104038

Zhu, K., Hopwood, M. J., Groenenberg, J. E., Engel, A., Achterberg, E. P., and Gledhill, M. (2021b). Influence of pH and Dissolved Organic Matter on Iron Speciation and Apparent Iron Solubility in the Peruvian Shelf and Slope Region. *Environ. Sci. Technol.* 55, 9372–9383. doi: 10.1021/ACS.EST.1C02477

**Conflict of Interest:** The authors declare that the research was conducted in the absence of any commercial or financial relationships that could be construed as a potential conflict of interest.

**Publisher's Note:** All claims expressed in this article are solely those of the authors and do not necessarily represent those of their affiliated organizations, or those of the publisher, the editors and the reviewers. Any product that may be evaluated in this article, or claim that may be made by its manufacturer, is not guaranteed or endorsed by the publisher.